Numerical study of domain coarsening in anisotropic stripe patterns

Denis Boyer*

Instituto de Física, Universidad Nacional Autónoma de México, Apartado Postal 20-364, 01000 Mexico City, Mexico
(Received 3 February 2004; published 4 June 2004)

We study the coarsening of two-dimensional smectic polycrystals characterized by grains of oblique stripes with only two possible orientations. For this purpose, an anisotropic Swift-Hohenberg equation is solved. For quenches close enough to the onset of stripe formation, the average domain size increases with time as $t^{1/2}$. Further from onset, anisotropic pinning forces similar to Peierls stresses in solid crystals slow down defects, and growth becomes anisotropic. In a wide range of quench depths, dislocation arrays remain mobile and dislocation density roughly decays as $t^{-1/3}$, while chevron boundaries are totally pinned. We discuss some agreements and disagreements found with recent experimental results on the coarsening of anisotropic electroconvection patterns.

PACS number(s): 64.60.Cn, 47.54.+r, 61.30.Jf

I. INTRODUCTION

Coarsening occurs when a system is rapidly quenched below a transition point into a phase with broken symmetries. The spatiotemporal evolution following a quench is relatively well known when the broken symmetry phase is characterized by a local order parameter that is spatially uniform (e.g., the local magnetization of a ferromagnetic phase [1,2]). The growth of spatial correlations, driven by domain growth or the annihilation of topological defects, usually obeys a dynamical scaling relation and the correlation length, or "domain size" R, grows as a power law of time with a well defined exponent. Classification schemes have been established for the main different cases [2,3].

The situation is much less understood for phases characterized by a local order parameter that is spatially modulated. Systems forming periodic patterns (stripes, hexagons) with a well defined periodicity can be observed in numerous physical systems, such as Rayleigh-Bénard convection, diblock-copolymer melts, magnetic materials, or Turing reaction-diffusion systems [4]. After a quench into a stripe phase, two-dimensional configurations are composed of many domains differently oriented, including grain boundaries, dislocations, and disclinations. Numerical [5–13] as well as experimental [14–17] studies have established that it is difficult, if not impossible, to reduce the ordering dynamics of stripes to one of the class known for uniform phases. There is still some debate regarding the growth mechanisms, the value of the growth exponent, whether dynamical scaling holds or not, or whether the system may involve various characteristic length scales growing with different exponents. In contrast with uniform phases, the coarsening rates depend significantly on the quench depth. Far away from the bifurcation threshold of stripe formation (large quenches), numerical solutions of the Swift-Hohenberg equation show that coarsening stops at large time, i.e., the system remain frozen in macroscopically disordered configurations [8,12]. Based on an analysis of the law of motion of a grain boundary

through curved stripes, it was recently proposed that a single growth exponent could be introduced, but for vanishingly small quenches only [11,12]. From dimensional arguments, a $R \sim t^{1/3}$ growth law was derived in that regime, in good agreement with numerical results at small quenches [11–13]. The freezing observed at finite quenches was attributed to the presence of a periodic pinning potential (generated by the pattern itself) acting on grain boundaries.

In the present paper, we consider a closely related problem where similar questions remain open, and that has not been investigated numerically so far: the coarsening of *anisotropic* stripe patterns. Oblique rolls making only two possible angles (θ or $-\theta$, fixed) with respect to a particular axis can be observed in electroconvection of nematic liquid crystals [4]. Studying the ordering dynamics on this system is motivated by various reasons. First, one can intend a comparison with available experimental data, since coarsening experiments have been recently conducted in electroconvection [14,15]. Second, the polycrystalline structures of oblique stripes have a relatively simpler geometry than those of isotropic stripes: the constraint of the fixed angle prevents the formation of disclinations. Therefore, the topological defects are essentially dislocations and (chevron) grain boundaries separating domains differently oriented. This situation can be seen as a smectic analog of the structures formed by grains in polycrystalline solids, where disclinations are also absent [18].

We consider in the following an extension of the Swift-Hohenberg equation for oblique stripes in two spatial dimensions. This model, proposed by Pesch and Kramer for describing electroconvection [19], is recalled in Sec. II. In Sec. III, we investigate *small* quenches: the numerical results show that coarsening is driven by surface tension and a growth law $t^{1/2}$ is observed for various characteristic length scales, like in model A [3]. The results qualitatively change at larger quenches (Sec. IV): the characteristic length scales associated with dislocations and chevron boundaries start to evolve differently, and the associated effective growth exponents progressively decrease as the quench depth increases. However, the effective exponent of the dislocation density remains fairly constant for a relatively wide range of quench depths. This feature can be explained by the fact that dislo-

---

*Electronic address: boyer@fisica.unam.mx

cations have a much lower pinning potential than chevron boundaries. We qualitatively justify this feature from weakly nonlinear analysis arguments. The dislocation exponent is close to the value of $1/3$ in that intermediate range, in agreement with the value measured in recent experiments [15]. Some conclusions are presented in Sec. V.

II. MODEL EQUATION

Electroconvection in nematic liquid crystals is a paradigm of anisotropic pattern formation [20]. If nematics is placed between two glass plates properly treated, its director can be aligned along a preferential direction, say the x axis. When an external ac electric field is applied in the direction normal to the plane, periodic rolls appear above a threshold. As the voltage is increased (the frequency being fixed in some proper range), bifurcations to various phases can be observed: "normal" rolls, with a wave vector directed along the x axis, usually appear first. This phase can be followed by a transition to "oblique" rolls, of interest here, characterized by a wave vector with two possible orientations with respect to the x axis, θ and $-\theta$.

Although the theoretical understanding of electroconvection patterns based on constitutive equations is still incomplete, some nonlinear models that rely on equations for a local order parameter and on symmetry arguments have been proposed. Some time ago, Pesch and Kramer introduced an anisotropic model [19] that exhibits a transition from normal to oblique rolls:

$$\frac{\partial \psi}{\partial t} = r\psi - \zeta^4(\Delta + k_0^2)^2\psi - \frac{c}{k_0^4}\partial_y^4\psi + \frac{2\eta}{k_0^4}\partial_x^2\partial_y^2\psi - \psi^3 \quad (1)$$

with $\partial_{x(y)} = \partial/\partial x(y)$. In Eq. (1), $\psi(\vec{x},t)$ is a local dimensionless order parameter, interpreted as a small lateral elastic displacement; c and η are dimensionless constants modeling the loading forces and anisotropic bending constants; k_0 is the wave number of the base periodic pattern, and ζ a "coherence" length that will be set to $1/k_0$ for simplicity here. The dimensionless parameter r is chosen as the main control parameter. For $c = \eta = 0$ the above equation reduces to the well known Swift-Hohenberg model of Rayleigh-Bénard convection (r is the reduced Rayleigh number in that case). The model (1) derives from a Liapunov "free-energy" functional. It can be recast as

$$\frac{\partial \psi}{\partial t} = -\frac{\delta F}{\delta \psi} \quad (2)$$

with

$$F = \frac{1}{2k_0^4}\int d\vec{r}[k_0^4(-r\psi^2 + \psi^4/2) + \psi(k_0^2 + \Delta)^2\psi - 2\eta(\partial_x\partial_y\psi)^2$$
$$+ c(\partial_y^2\psi)^2]. \quad (3)$$

The functional F monotonically decreases with time, $dF/dt \leq 0$.

Linear stability analysis of Eq. (1) around the state $\psi(\vec{x},t) = 0$ shows that two modes of finite wave number $\vec{k} = p\hat{x} + q\hat{y}$ ($\hat{x}$ and $\hat{y}$ are unitary vectors) become marginally unstable when the control parameter r increases and crosses some threshold values $r_c^{(o)}$ and $r_c^{(n)}$,

$$r_c^{(o)} = \frac{-\eta^2}{c + 2\eta - \eta^2} < 0, \quad \left\{ p_c^2 = \frac{k_0^2(c + \eta)}{c + 2\eta - \eta^2}, \right.$$
$$\left. q_c^2 = \frac{k_0^2\eta}{c + 2\eta - \eta^2} \right\} \quad \text{(oblique rolls)}, \quad (4)$$

$$r_c^{(n)} = 0, \quad \{p_c^2 = k_0^2, \quad q_c^2 = 0\} \quad \text{(normal rolls)}. \quad (5)$$

In the above relations, we have considered the case $c > 0$, the condition for which the instability at $r_c = 0$ is to normal rolls ($p_c = 0$). In the oblique phase, rolls make an angle $\theta = \pm\arctan[\sqrt{\eta/(c+\eta)}]$ with the y axis. As obvious from Eq. (4), oblique rolls can only be observed for $\eta > 0$. Hence, when η is tuned from negative to positive values, a transition form normal to oblique rolls can occur. In order to study the coarsening of oblique rolls, we will choose $c > 0$ and $\eta > 0$ in the following.

Oblique rolls have the lowest threshold value ($r_c^{(o)} < 0$) and we renote $r_c \equiv r_c^{(o)}$ for simplicity. As already noted by Pesch and Kramer, the structures that are likely to be observed for r in the range $[r_c, 0]$ may not be oblique rolls, but more complicated, nonlinear structures ("undulated" rolls) that are not of interest here. When numerically solving Eq. (1) with random initial conditions and $r_c \leq r \leq 0$, we actually observed that oblique rolls never appeared. On the other hand, configurations of oblique rolls very similar to those observed experimentally [14,15] are always observed when setting $r > 0$ instead. Normal rolls were never observed in the runs presented in the following sections. This is consistent with the weakly nonlinear analysis of Eq. (1) that predicts that oblique rolls have a lower free energy F [19]. Therefore, we define the quench depth as

$$\epsilon = r - r_c, \quad (6)$$

with r_c given by Eq. (4). We always choose ϵ larger than $|r_c|(r > 0)$.

III. COARSENING KINETICS NEAR ONSET ($\epsilon \ll 1$)

We numerically solve Eq. (1) by using a pseudospectral method and a time integration procedure whose descriptions can be found in Ref. [21]. The space is discretized on a square lattice of 1024^2 nodes with a lattice size Δx set to unity. The base period $\lambda_0 \equiv 2\pi/k_0$ of the pattern is fixed to $8\Delta x$. The time integration scheme is stable for relatively large value of the time step, which is fixed to 0.5 in dimensionless time units. The initial condition for ψ is a random field with Gaussian distribution, of zero mean and variance $\sqrt{\epsilon/3}$.

Figure 1 displays in gray scale the order parameter ψ at time $t = 1200$ time units, for a run with $c = 12$ and $\eta = 0.5$ (the angle of the rolls with the vertical axis is $11.31°$). The quench depth is *small*, and has been set to $\epsilon = 1.9|r_c| \simeq 0.0372$. The configuration is that of a smectic polycrystal: Most of the defects present are grain boundaries separating zig and zag rolls, and few isolated dislocations can be ob-
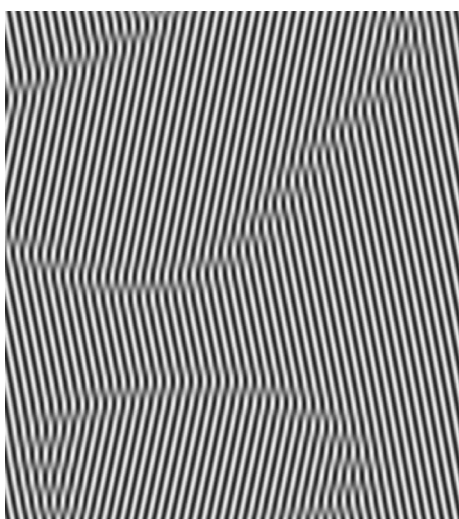
FIG. 1. Local order parameter in gray scale (detail), $c=12$, $\eta=0.5$, $\epsilon=0.0372$, $t=1200$, obtained from random initial conditions.

served. Due to the asymmetry of the problem, two kind of boundaries can be roughly distinguished: "horizontal" chevron boundaries where the roll orientation changes rather smoothly from one grain to the other, and "vertical" (or inclined) boundaries, which are made of dense arrays of dislocations. This distinction is not very sharp, as one goes continuously from one situation to the other, corresponding to boundaries of "low" and "high" dislocation density, respectively. The defect field shown in Fig. 2 is obtained from Fig. 1 by using a Fourier filtering procedure. The dark areas correspond to defected regions. Dislocations tend to be distributed along stringlike structures, like in crystals.

At very large times, grain boundaries are weakly curved and isolated dislocations lying inside a grain are relatively rare. These observations agree with recent electroconvection experiments [15], where a mechanism for the formation of isolated dislocations was identified: A shrinking bubble can be roughly pictured as delimited by two vertical and two

FIG. 2. Defects (marked in black) of a configuration with same parameters as in Fig. 1, at a larger scale.
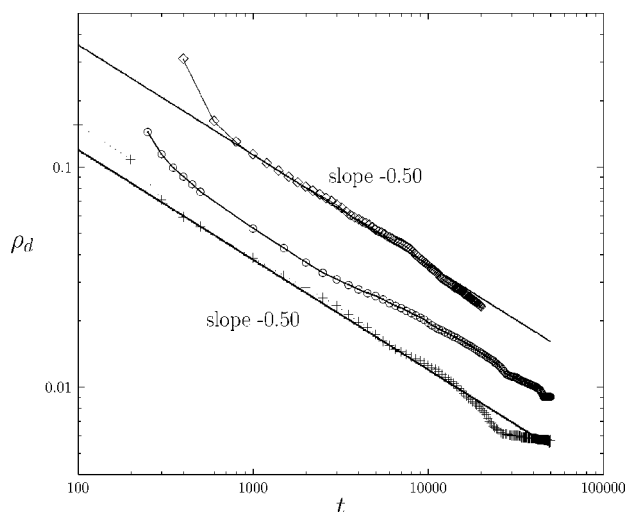

FIG. 3. Defect density as a function of time. From bottom to top. (+) symbols, $c=12$, $\eta=0.5(\theta=11.31°)$, $\epsilon=1.9|r_c|=0.0372$; ($\diamond$) symbols, $c=6$, $\eta=0.25(\theta=11.31°)$, $\epsilon=1.9|r_c|=0.0184$; ($\bigcirc$) symbols, $c=3$, $\eta=0.25(\theta=15.50°)$, $\epsilon=1.9|r_c|=0.0345$. Average are performed over 13 runs in each case. Solid lines are guides to the eye.

horizontal grain boundaries. In some cases, the two vertical boundaries are not composed by the same number of dislocations, therefore, some dislocations cannot annihilate with others of opposite Burgers vector when the bubble shrinks. However, this situation occurs rarely.

We study the time evolution of the defect density ρ_d, defined as the fraction of area occupied by the black regions in Fig. 2. We perform three series of runs at small quenches, each satisfying $\epsilon=1.9|r_c|$ for different choices of the parameters $\{c,\eta,r\}$ ($\epsilon=0.0372, 0.0184, 0.0345$, respectively). Figure 3 shows a summary of the data obtained. In each case, the results are consistent with the law

$$\rho_d \sim t^{-1/2}, \qquad (7)$$

which corresponds to a defect characteristic length scale growing as $t^{1/2}$. This result seems to be fairly independent of the angle θ.

We next investigate the time evolution of the Liapunov functional F given by Eq. (3). If F_0 denotes the value of F for a perfectly ordered system, then the quantity $\Delta F=F-F_0$ represents the excess energy due to defects. The system free energy F decreases like the total length of grain boundaries. From Eq. (7), one should expect

$$F - F_0 \sim t^{-1/2}. \qquad (8)$$

The numerical data plotted in Fig. 4 for small values of ϵ are consistent with this scaling relation as well.

The time evolution of many coarsening systems is self-similar: the large scale structure of successive configurations is statistically time invariant, provided that spatial variables
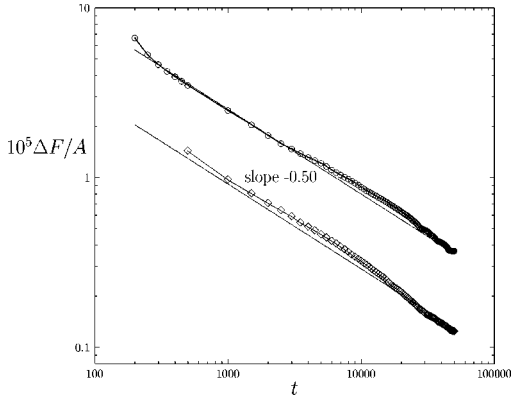
FIG. 4. Relative Liapunov free-energy per unit area (A is the system area) as a function of time. The legend is the same as in Fig. 3. Solid lines are guides to the eye.

are rescaled by a proper length. We thereby analyze the structure factor, defined as the Fourier transform of the two-point correlation function, $S(\vec{k}) = \langle \psi(\vec{k},t)\psi(-\vec{k},t) \rangle$, the braces representing average over initial conditions. $S(\vec{k})$ is maximum for any of the (four) wave vectors $\vec{k}_Z$ characterizing zig and zag rolls. At any given time, we numerically observe that S is maximal for $\vec{k}_Z \approx \vec{k}_c$, given by Eq. (4). Therefore, the selected stripe periodicity and orientation in the polycrystalline structure are that of the marginal wave vectors $\vec{k}_c$ determined from linear stability analysis. A similar situation is encountered for the isotropic Swift-Hohenberg model, and is thought to be more generally a property of potential systems [7]. Near any peak $\vec{k}_Z$ of S, we propose the following scaling ansatz:

$$S(\delta k_\parallel, \delta k_\perp, t) = \xi_\parallel(t)\xi_\perp(t)f[\xi_\parallel(t)\delta k_\parallel, \xi_\perp(t)\delta k_\perp], \quad (9)$$

where $\delta\vec{k} = \vec{k} - \vec{k}_Z = \delta k_\parallel \hat{k}_\parallel + \delta k_\perp \hat{k}_\perp$, with $\hat{k}_\parallel$ and $\hat{k}_\perp$ denoting the unit vectors longitudinal and transverse to the wave vector $\vec{k}_Z$, respectively. $f(x)$ is a scaling function, $\xi_\parallel(t)$ and $\xi_\perp(t)$ are *a priori* two characteristic lengths describing grain growth in the directions normal and parallel to the rolls, respectively. Let us define $S_\parallel(\delta k_\parallel, t) \equiv \int_{-\infty}^{\infty} \delta k_\perp S(\delta\vec{k}, t)$, a symmetric relationship defining $S_\perp$. From Eq. (9), one obtains the scaling ansatz

$$S_\parallel(\delta k_\parallel, t) = \xi_\parallel(t)g[\xi_\parallel(t)\delta k_\parallel]. \quad (10)$$

Figure 5 displays $S_\parallel$ as a function of $\delta k_\parallel$ at various times ($t = 5\times 10^2, 2\times 10^3, 5\times 10^3, 5\times 10^4$), for $\{c = 6, \eta = 0.25, \epsilon = 1.9|r_c|\}$. The scaling relation (10) holds over nearly two decades, despite a slight widening at large times. The length $\xi_\parallel(t)$, taken from the maximum value of $S_\parallel$ is plotted as a function of time in Fig. 6. The results are in good agreement with

$$\xi_\parallel(t) \sim t^{1/2}. \quad (11)$$

We have not found $\xi_\perp(t)$, determined from $S_\perp$, to be a convenient length scale to characterize coarsening. $\xi_\perp$ is larger than $\xi_\parallel$ by a factor varying between 5 (at short times) and 2
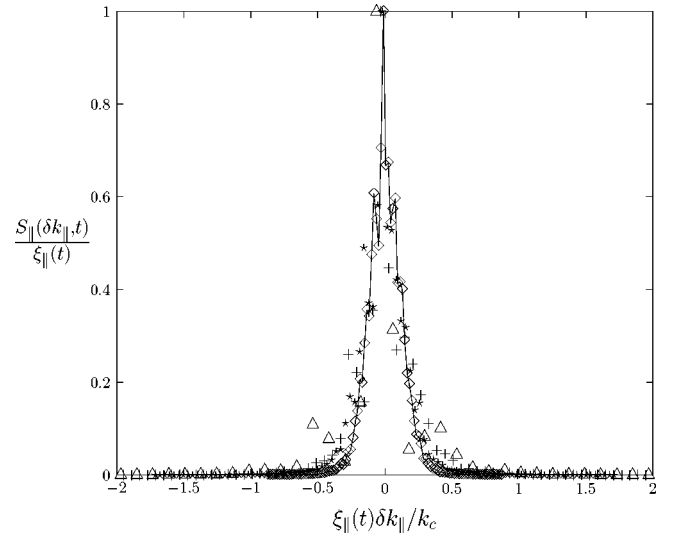

FIG. 5. Structure factor $S_\parallel(\delta k_\parallel, t)$ at four different times: $t = 5\ 10^2(\diamond), 2\ 10^3(*), 5\ 10^3(+), 2\ 10^4(\triangle)$. At each time, the curve has been rescaled according to Eq. (10), where $\xi_\parallel(t)$ is defined as $S(\delta k_\parallel = 0, t)$. The parameters are $c = 6, \eta = 0.25, \epsilon = 1.9|r_c|$. (Averages over 40 independent runs.)

(at large times). This could be due to some phase correlations of longer range than those associated with domain walls; these features were not investigated.

The above results are consistent with a coarsening process driven by grain boundary surface tension and involving a single characteristic length scale, like for the dynamics of model A for a nonconserved order parameter [3]. The law $R \sim t^{1/2}$ is also expected to describe the kinetics of grain growth in solid polycrystals [22]. This situation differs markedly from isotropic stripes (where $R \sim t^{1/3}$ [11–13]). Note that the available experimental studies on anisotropic stripes have reported much slower coarsening laws than Eq. (11), namely, $t^{1/5}$ or $t^{1/4}$ [14,15].
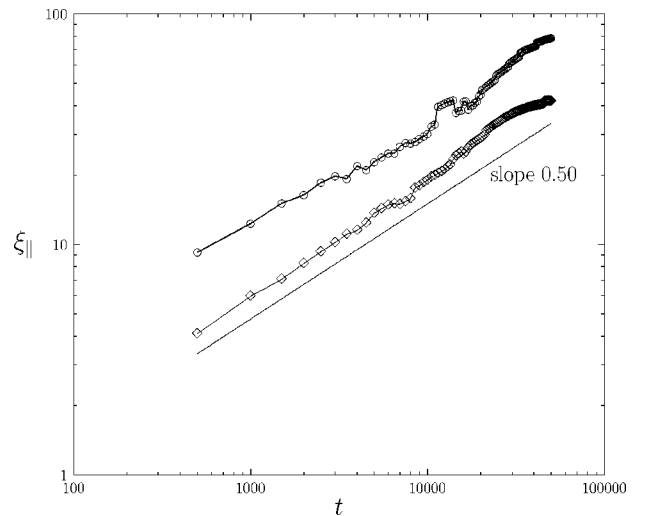

FIG. 6. Length determined from the maximal intensity of the structure factor. See Fig. 3 for legends. The solid line is a guide to the eye.
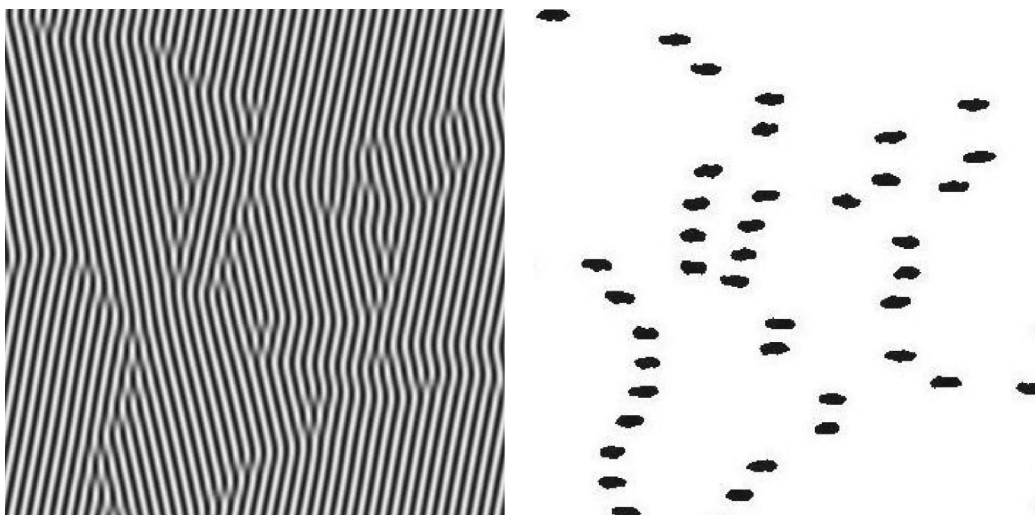
FIG. 7. (a) Local order parameter in gray scale, $c=12$, $\eta=0.5$, $t=500$. The quench is "moderate": $\epsilon=11|r_c|=0.215$. The chevron boundaries are now straight and pinned. (b) Dislocation field of (a) (same scale) obtained with the Fourier filtering procedure.

IV. COARSENING AT LARGER QUENCH DEPTHS

A. Phenomenology of pinning forces in modulated phases

In solid crystals, for an isolated dislocation to glide from one row of atoms to the next one, there is a finite energy cost corresponding to the rows that have to be compressed or dilated during the move. The resulting elastic force, the Peierls stress, tends to prevent the glide of dislocations [23,24]. Therefore, dislocations tend to be pinned in positions (periodically spaced) of minimum energy, and motion takes place only if an external stress larger than the critical Peierls stress is applied. Remarkably, the defects present in systems that form periodic patterns are also subjected to similar pinning forces. Their origin is nonlinear in that case, and is due to the apparition of "nonadiabatic" terms in weakly nonlinear expansions. Studies on the Swift-Hohenberg model have shown that the laws of motion of grain boundaries (or dislocation arrays) involve short range, spatially periodic pinning forces [12,25–27]. Either in crystals or in patterns, the law of motion of a defect takes the general form

$$\mu^{-1}v = \mu^{-1}dx/dt = f - p\,\cos(k_p x), \qquad (12)$$

where v is the defect velocity, x its position (for a grain boundary, the coordinate normal to the interface), μ a mobility, f an external force per unit length (e.g., the driving force for coarsening), and p the magnitude of the pinning force, which oscillates with a periodicity $2\pi/k_p$ proportional to the crystal (or base pattern) periodicity λ_c. Peierls-like pinning forces are usually much smaller than the other characteristic elastic forces (such as the critical threshold shear stress f_{cr}), and have the same general approximate expression, valid both for solids [23,24] and nonlinear patterns [12,25]:

$$p/f_{cr} \sim \exp[-aW/\lambda_c], \qquad (13)$$

where W is the width of the defect (see further Fig. 8), and a a constant of order unity. For instance, grain boundaries

separating domains of stripes have a width $W \sim \lambda_c/\sqrt{\epsilon}$ [27]. Therefore, close to the onset of the supercritical bifurcation ($\epsilon \to 0^+$), W becomes very large and the pinning potential (13) can be neglected. On the other hand, as the quench depth ϵ increases, W decreases and pinning forces can become large enough to affect qualitatively defect dynamics.

During a coarsening process driven by surface tension, the average force f in Eq. (12) is time dependent: $f \sim \gamma\kappa \sim \gamma/R(t)$, with γ and κ the typical interface surface tension and curvature, respectively. At short times, domains have small sizes R, and f is large compared with p in Eq. (12). Defects move easily and the average grain size grows. As a result, the driving force f decreases with time. At some point, f may eventually become lower than the typical value of p (which is time independent). In this case, boundaries become pinned at one of the discrete stable positions x_p such that $v=0$ in Eq. (12). This situation is easy to observe numerically
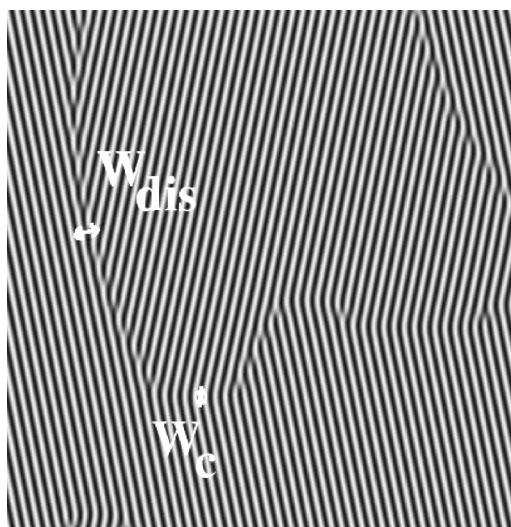

FIG. 8. Same parameters as in Fig. 7, at $t=50\,000$ (detail). The chevron boundaries and dislocations have a width W_c and W_{dis}, respectively.

for large quenches (p large), where asymptotic patterns remain only partially ordered ("glassy"), with many immobile defects [8,12]. On the other hand, in the regime $\epsilon \rightarrow 0$, defect pinning is negligible during the numerical time scales studied, and coarsening dynamics is more likely to be self-similar and characterized by well defined exponents.

For intermediate quenches, well before all grain boundaries of a system become pinned, the Peierls-like barriers are believed to slow down the ordering kinetics. At intermediate times, one may still be able to fit in some cases the numerical results with power laws, $R \sim t^{1/z^*}$. z^* now represents an *effective* growth exponent, and $z^* \geq z|_{\epsilon \rightarrow 0}$.

B. Pinning of anisotropic stripes

To check whether the arguments presented above apply to anisotropic patterns as well, we have performed calculations for deeper quenches than in Sec. III.

Figure 7(a) shows in gray scale the field ψ of a fraction of the system, obtained for a "moderate" quench of depth $\epsilon = 11|r_c| = 0.215$, at time $t = 500$ with $\{c = 12, \eta = 0.5\}$. The two classes of defects previously mentioned, the horizontal chevron grain boundaries and the dislocations, can now be clearly distinguished. [The dislocation field is shown in Fig. 7(b)]. The chevron boundaries are fairly straight. They remain practically immobile during the whole coarsening process, which is driven by dislocation motion only. This feature was observed in experiments as well [14,15]. A detail of a large time configuration ($t = 50\,000$) is shown in Fig. 8. Like for shallow quenches, dislocations tend to organize along string-like structures that are generally curved. We interpret the immobility of the chevron boundary as caused by strong pinning forces. Given two domains of zig and zag rolls, the stable positions of a chevron boundary are imposed by the phase of the local order parameter, which does not change across the boundary when one follows a given roll. On the other hand, dislocations are much more mobile, suggesting that their pinning potential p is very low, and therefore strongly anisotropic with respect to the grain boundary orientation.

In the following, we define the effective exponents associated with dislocations, free-energy and structure factor, respectively:

$$\rho_{dis} \sim t^{-1/z_{dis}^*}, \quad \Delta F \sim t^{-1/z_F^*}, \quad \xi_{\parallel}(t) \sim t^{1/z_S^*}, \quad (14)$$

where ρ_{dis} is the dislocation density, and is determined the same way as ρ_d in Sec. III [the fraction of black area of Fig. 7(b)] [28]. The other quantities have been defined in Sec. III.

We have plotted the time evolution of the relative free-energy per unit area ΔF in Fig. 9, for different quench depths. Similar curves are obtained for the dislocation density ρ_{dis} (Fig. 10), and the correlation length ξ (not shown). Provided that $\epsilon \leq 35|r_c|$, the curves are still reasonably well fitted by power laws during the first few decades considered in the numerical calculations. At larger quenches, they rapidly saturate a finite value indicating defect pinning. In these cases, we define the effective exponent (arbitrarily) as given at time $t = 1000$,
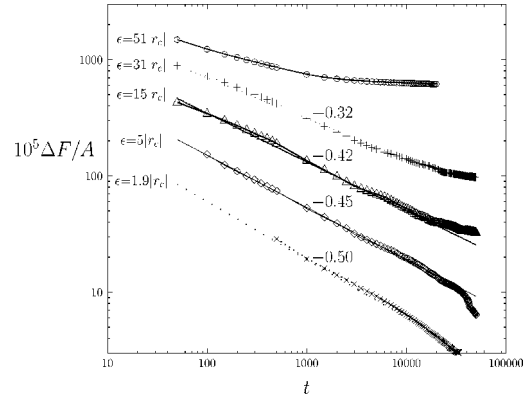

FIG. 9. Relative free energy per unit area as a function of time for $c = 12$, $\eta = 0.5$ and various quench depths. From bottom to top: $\epsilon = 0.037; 0.098; 0.294; 0.607; 1$.

$$z_{dis}^* = - \left(\left. \frac{d \ln \rho_{dis}}{d \ln t} \right|_{t=1000} \right)^{-1} \quad (15)$$

(and similar relations for z_F^* and z_S^*).

As expected from the discussion of Sec. IV A, the ordering kinetics slow down noticeably as ϵ is increased. All exponents z_{dis}^*, z_F^*, and z_S^* increase with ϵ. Figure 11 displays the variations of the different effective exponents as a function of ϵ. The dislocation exponent z_{dis}^* differs noticeably from z_F^* (and z_S^*): $z_{dis}^* > z_F^* > z_S^*$. The behavior of z_F^* is characterized by two regimes: At moderate quenches, z_F^* gradually departs from $z_F^* = 2$ and slowly increases with ϵ up to a value close to 3. For $\epsilon \gtrsim 35|r_c|$, z_F^* then increases more sharply, the signature of a sudden increase of pinning effects. A similar behavior (although less pronounced) is observed for z_S^*. The behavior of z_{dis}^* with the quench depth is more abrupt. The variations of z_{dis}^* are quite important for small and large values of ϵ. The most striking feature is the presence of a fairly long plateau at intermediate quenches ($5|r_c| < \epsilon < 35|r_c|$) where z_{dis}^* remains practically constant, $z_{dis}^* \simeq 3$. This result
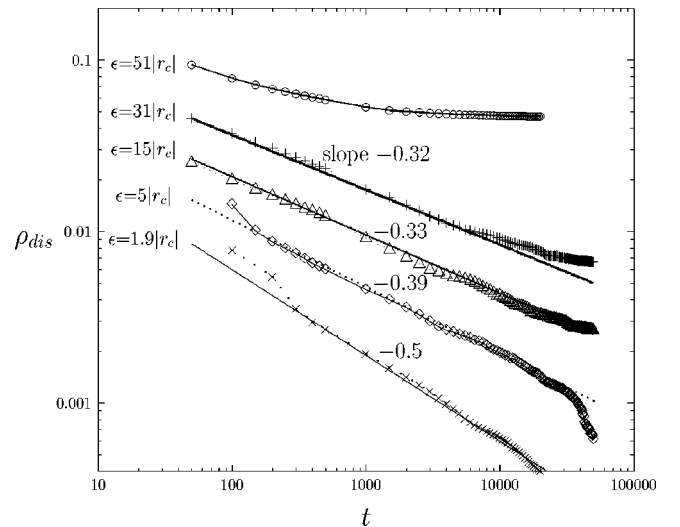

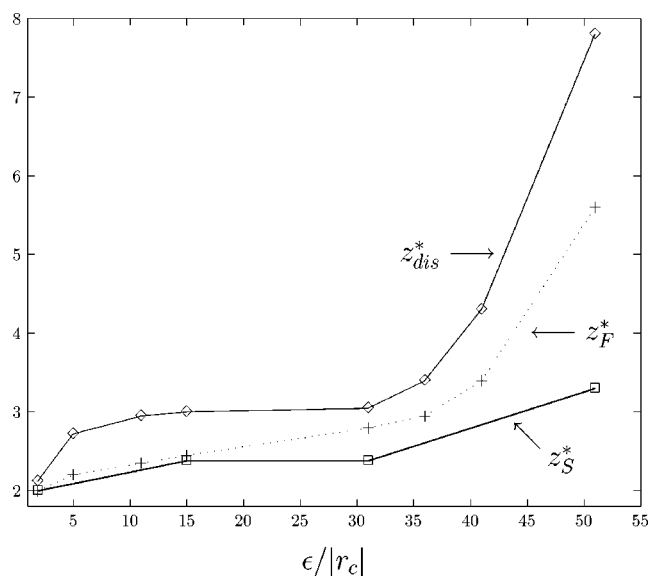FIG. 10. Dislocation density as a function of time. Same parameter as in Fig. 9.

FIG. 11. Effective exponents for dislocations, energy, and structure factor as a function of the reduced quench depth $\epsilon/|r_c|$. The parameters in Eq. (1) are $c=12$, $\eta=0.5$.

agrees with the experimental results of [15], where a law $t^{-1/3}$ was reported for the dislocation density.

C. Discussion

We sketch a possible interpretation of part of the above observations, based on the fact that pinning effects are strongly anisotropic. We saw that, away from onset, chevron boundaries become totally pinned. Meanwhile, dislocations are mobile and may still have a very low pinning potential. From the standard relation for the width of a grain boundary in stripe patterns, derived from weakly nonlinear analysis [27], let us assume that the width of chevron boundaries (W_c) and that of a roughly vertical dislocation array (W_{dis}, see Fig. 8) are given by $W_{c,dis}=\delta_{c,dis}\lambda/\sqrt{\epsilon}$, with δ_c and δ_{dis} two constants of order unity. From observations, let us assume that dislocations have a larger width than chevrons: $W_{dis}>W_c$, i.e., $\delta_{dis}>\delta_c$.

From the general relation (13), the pinning potentials have a nonanalytical behavior at low ϵ, and saturate at large ϵ ($p\sim\exp[-cst/\sqrt{\epsilon}]$). If $\delta_{dis}>\delta_c$, the pinning potentials p_c and p_{dis} for chevrons and dislocations, respectively, are such that $p_{dis}\ll p_c\ll 1$ if $\epsilon\ll 1$. A moderate increase of ϵ can cause a rapid increase of p_c up to its saturation value, while p_{dis} may still remain very low. This situation can happen in the range of quench depths defined by $(a\delta_c)^2<\epsilon<(a\delta_{dis})^2$ [a is introduced in Eq. (13)], provided that this range is sufficiently broad. Hence, one would expect the coarsening dynamics to

be relatively insensitive to the value of ϵ in that range, as observed numerically for $5|r_c|<\epsilon<35|r_c|$ in Fig. 11. Further increase of ϵ eventually produces dislocation pinning, and a general slowing down of the system must occur: it is illustrated by the inflection of the effective exponents past $35|r_c|$.

Let us assume next that the system is described by two characteristic length scales, L_{dis} and L_c, representing the linear extent of a grain along the y and x directions, respectively. Following the arguments of Ref. [15], the dislocation density can be written as $\rho_{dis}\sim L_{dis}/(L_{dis}L_c)=L_c^{-1}$. In the moderate quench regime ($5|r_c|<\epsilon<35|r_c|$), $L_c\sim t^{1/3}$. In this regime, the results on the energy and the structure factor (Fig. 11) suggest that the other length scale L_{dis} grows faster than $t^{1/3}$ ($2\leq z^*\leq 3$). Therefore, as time goes, defected regions tend to be more composed of dislocations than chevron boundaries ($L_{dis}>L_c$). Unfortunately, this finding disagrees with the experimental results on electroconvection, where the opposite behavior was found: a very slow growth law for L_{dis} ($\sim t^{1/5}$), as well as a similar law for a correlation length, was reported in Ref. [15]. Hence, the experimental grains are elongated along the x direction at late stages [29].

V. CONCLUSIONS

We have presented evidence that the coarsening of smectic patterns, as given by a potential anisotropic Swift-Hohenberg equation, is characterized by a $t^{1/2}$ law close to onset. This law has not been observed experimentally so far in electroconvection of nematic liquid crystals, and may correspond to a regime difficult to reach. For larger quench depths, the phase ordering kinetics is affected by pinning effects that strongly depend on grain boundary orientations. A particular regime is observed numerically for a fairly wide interval of moderate quenches: chevron boundaries get pinned, and grain growth still takes place via mobile arrays of dislocations. A similar behavior was observed in experiments [14,15]. In this regime, the dislocation density behaves as $t^{-1/3}$, the same decay rate as found experimentally [15]. Our results suggest that the characteristic length of a dislocation array grows faster than that of a chevron boundary. This feature disagrees with the experimental findings, though, and may point out a limitation of the present model. Nonpotential effects, which have been neglected here, probably play an important role in this system.

[1] J. Gunton, M. San Miguel, and P. Sahni, in *Kinetics of First Order Phase Transitions*, edited by C. Domb and J. Lebowitz, Phase Transitions and Critical Phenomena, Vol. 8 (Academic, London, 1983).

[2] A. Bray, Adv. Phys. **43**, 357 (1994).

[3] P. Hohenberg and B. Halperin, Rev. Mod. Phys. **49**, 435 (1977).

[4] M. C. Cross and P. C. Hohenberg, Rev. Mod. Phys. **65**, 851 (1993).

[5] K. R. Elder, J. Viñals, and M. Grant, Phys. Rev. Lett. **68**, 3024 (1992).

[6] K. R. Elder, J. Viñals, and M. Grant, Phys. Rev. A **46**, 7618 (1992).

[7] M. C. Cross and D. I. Meiron, Phys. Rev. Lett. **75**, 2152 (1995).

[8] Q. Hou, S. Sasa, and N. Goldenfeld, Physica A **239**, 219 (1997).

[9] Y. Shiwa, T. Taneike, and Y. Yokojima, Phys. Rev. Lett. **77**, 4378 (1996).

[10] J. J. Christensen and A. J. Bray, Phys. Rev. E **58**, 5364 (1998).

[11] D. Boyer and J. Viñals, Phys. Rev. E **64**, 050101 (2001).

[12] D. Boyer and J. Viñals, Phys. Rev. E **65**, 046119 (2002).

[13] H. Qian and G. F. Mazenko, Phys. Rev. E **67**, 036102 (2003).

[14] L. Purvis and M. Dennin, Phys. Rev. Lett. **86**, 5898 (2001).

[15] C. Kamaga, F. Ibrahim, and M. Dennin, e-print cond-mat/0404117.

[16] C. Harrison *et al.*, Science **290**, 1558 (2000).

[17] C. Harrison, Z. Cheng, S. Sethuraman, D. A. Huse, P. M. Chaikin, D. A. Vega, J. M. Sebastian, R. A. Register, and D. H. Adamson, Phys. Rev. E **66**, 011706 (2002).

[18] P. Chaikin and T. Lubensky, *Principles of Condensed Matter Physics* (Cambridge University Press, New York, 1995).

[19] W. Pesch and L. Kramer, Z. Phys. B: Condens. Matter **63**, 121 (1986).

[20] S. Kai, N. Chizumi, and M. Kohno, Phys. Rev. A **40**, 6554 (1989).

[21] M. Cross, D. Meiron, and Y. Tu, Chaos **4**, 607 (1994).

[22] W. W. Mullins, J. Appl. Phys. **27**, 900 (1956).

[23] R. E. Peierls, Proc. Phys. Soc. London **52**, 34 (1940).

[24] F. R.N. Nabarro, *Theory of Crystal Dislocations* (Dover, New York, 1987).

[25] D. Boyer and J. Viñals, Phys. Rev. Lett. **89**, 055501 (2002).

[26] Y. Pomeau, Physica D **23**, 3 (1986).

[27] B. A. Malomed, A. A. Nepomnyashchy, and M. I. Tribelsky, Phys. Rev. A **42**, 7244 (1990).

[28] The filtering procedure is such that, at as soon as $\epsilon \gtrsim 5|r_c|$, dislocations only are emphasized, while the extended chevron boundaries, previously visible in Fig. 2 at shallow quenches, no longer appear. Therefore, in the moderate-large quench regime, the defect density determined from filtering has to be identified with ρ_{dis} only, and no longer with the total amount of defects of the system ρ_d (dislocations+chevron boundaries).

[29] C. Kamaga (private communication).